

OPEN ACCESS

EDITED BY

Xi Wang, The Chinese University of Hong Kong, Hong Kong SAR, China

REVIEWED BY

Junmena Li.

Henan Provincial People's Hospital, China Xiang-Xu Wang,

Air Force Medical University, China

*CORRESPONDENCE

Ziqiao Lei

⊠ ziqiao_lei@hust.edu.cn

Xiangchuang Kong

M hongke80@hust.edu.cn

Guofeng Zhou

[†]These authors have contributed equally to

RECEIVED 03 September 2025 REVISED 25 October 2025 ACCEPTED 07 November 2025 PUBLISHED 28 November 2025

CITATION

Wang Y, Jiang S, Yang Y, Li Y, Li Z, Lei Z, Kong X and Zhou G (2025) Prediction of long-term survival in gastric cancer patients after immunotherapy based on CT-derived extracellular volume fraction. *Front. Oncol.* 15:1698065. doi: 10.3389/fonc.2025.1698065

COPYRIGHT

© 2025 Wang, Jiang, Yang, Li, Li, Lei, Kong and Zhou. This is an open-access article distributed under the terms of the Creative Commons Attribution License (CC BY). The use, distribution or reproduction in other forums is permitted, provided the original author(s) and the copyright owner(s) are credited and that the original publication in this journal is cited, in accordance with accepted academic practice. No use, distribution or reproduction is permitted which does not comply with these terms.

Prediction of long-term survival in gastric cancer patients after immunotherapy based on CT-derived extracellular volume fraction

Yuyang Wang^{1,2,3†}, Shanshan Jiang^{1,2,3†}, Yanjie Yang^{1,2†}, Yi Li^{1,2,3}, Zhiying Li⁴, Ziqiao Lei^{1,2,3*}, Xiangchuang Kong^{1,2,3*} and Guofeng Zhou^{1,2,3*}

¹Department of Radiology, Union Hospital, Tongji Medical College, Huazhong University of Science and Technology, Wuhan, China, ²Hubei Provincial Clinical Research Center for Precision Radiology and Interventional Medicine, Wuhan, China, ³Hubei Key Laboratory of Molecular Imaging, Wuhan, China, ⁴Department of Gastrointestinal Surgery, Union Hospital, Tongji Medical College, Huazhong University of Science and Technology, Wuhan, China

Background: Gastric cancer remains a leading cause of cancer-related mortality. While immune checkpoint inhibitors (ICIs) have emerged as promising therapies, their efficacy is hindered by the lack of robust patient-centric biomarkers. CT-derived extracellular volume fraction (ECV) has emerged as a novel approach for non-invasive quantification of the extracellular matrix (ECM). This study assesses the predictive value of ECV, a non-invasive imaging biomarker, in gastric cancer patients receiving programmed death receptor-1 (PD-1) inhibitors.

Methods: A retrospective study was conducted on 101 gastric adenocarcinoma patients (stage III: n=47; stage IV: n=54) treated with PD-1 inhibitors at Wuhan Union Hospital from June 21, 2020 to January 3, 2024. The patients were stratified into high- and low-ECV groups using X-tile software. Survival outcomes were compared using Kaplan–Meier curves and log-rank tests. Cox regression analyses identified independent prognostic factors. Two predictive models were developed and evaluated via receiver operating characteristic (ROC) curves and area under the curve (AUC), with internal validation using 1,000 bootstrap iterations.

Results: Kaplan–Meier survival curves indicated that the ECV-higher group had shorter progression-free survival (PFS) (P < 0.001) and overall survival (OS) (P < 0.001) than the ECV-lower group. Multivariate Cox regression analysis confirmed that high CT-ECV was independently associated with worse PFS and OS (PFS: HR = 2.716, 95% CI: 1.432–5.152, P = 0.002 and OS: HR = 2.593, 95% CI: 1.322–5.084, P = 0.006).

Conclusion: CT-derived ECV may serve as an independent predictor of long-term survival in gastric cancer patients undergoing immunotherapy.

KEYWORDS

gastric cancer, immunotherapy, PD-1 inhibitors, biomarkers, extracellular volume fraction, extracellular matrix, contrast-enhanced CT

Introduction

Gastric cancer is the fifth most common malignant tumor worldwide, with the 2024 statistics showing over 960,000 new cases annually and its ranking as the fifth leading cause of cancer-related deaths (1). In recent years, immune checkpoint inhibitors (ICIs), such as programmed cell death ligand-1 (PD-L1)/programmed death receptor-1 (PD-1) inhibitors, have significantly improved the survival outcomes for some advanced gastric cancer patients. However, existing biomarkers like PD-L1 expression, microsatellite instability (MSI), and Epstein-Barr virus (EBV) infection status, while partially predictive of therapeutic efficacy, exhibit high heterogeneity in expression influenced by tumor histotype, individual genetic background, and dynamic microenvironment changes (2). This results in most patients failing to benefit from immunotherapy, with some potentially experiencing worsened conditions due to immune-related adverse events (irAEs). Therefore, identifying novel biomarkers that overcome heterogeneity limitations has become an urgent need to optimize precision stratification in gastric cancer immunotherapy.

The extracellular matrix (ECM), a three-dimensional macromolecular network composed of collagens, proteoglycans/ glycosaminoglycans, elastin, fibronectin, laminins, several other glycoproteins, and various molecules (cytokines, growth factors, and hormones) (3), is essential for cellular functions including proliferation, migration, and differentiation through cell-ECM interactions (4). As a dynamic structure present in all tissues, ECM not only provides structural integrity but also maintains homeostasis through continuous remodeling in response to environmental stimuli (5, 6). Dysregulated ECM remodeling accelerates disease progression and tumor-associated ECM alterations promote tumor growth through tumor-stromal signaling, while increased matrix stiffness facilitates tumor invasion. This vicious cycle creates dense ECM barriers around tumor cells that physically impede drug penetration, reducing therapeutic efficacy (7, 8).

Traditional ECM assessment relying on invasive biopsy staining techniques (e.g., Masson staining) suffers from limitations in dynamic monitoring. Recently, radiomics-based extracellular volume fraction (ECV) technology has emerged as a novel approach for noninvasive ECM quantification. By calculating the distribution differences of intravenous contrast agents (e.g., iodinated contrast) in extracellular spaces, ECV indirectly reflects the ECM fibrosis degree and spatial distribution (9). Originally developed for cardiac fibrosis assessment (10), ECV has demonstrated value in evaluating liver cirrhosis and

Abbreviations: ICIs, immune checkpoint inhibitors; ECV, extracellular volume fraction; ECM, extracellular matrix; PD-1, programmed death receptor-1; ROC, receiver operating characteristic; AUC, area under the curve; PD-L1, programmed cell death ligand-1; MSI, microsatellite instability; EBV, Epstein–Barr virus; irAEs, immune-related adverse events; CECT, contrast-enhanced computed tomography; CA19-9, carbohydrate antigen 19-9; CEA, carcinoembryonic antigen; ROIs, regions of interest; ICC, intraclass correlation coefficient; SD, standard deviation; PFS, progression-free survival; OS, overall survival; HRs, hazard ratios;CIs, confidence intervals.

pancreatic fibrosis and predicting tumor regression grade after neoadjuvant therapy in gastric cancer and postoperative pancreatic complications (11–13). Multiple studies have validated ECV as a quantitative biomarker for ECM assessment in various solid tumors (14–18). Although ECV's potential in gastric cancer has gained attention (4, 19–23), its clinical translational value for predicting immunotherapy outcomes remains unclear. This study proposes using contrast-enhanced computed tomography (CECT) to measure ECV, aiming to quantify gastric cancer ECM fibrosis as a reflection of suppressive tumor immune microenvironment status, thereby predicting survival benefits from PD-1/PD-L1 inhibitor therapy.

Methods

Patients

A total of 195 patients with gastric adenocarcinoma who received PD-1 inhibitor immunotherapy at Wuhan Union Hospital between June 21, 2020 and January 3, 2024 were initially enrolled. All enrolled patients were treated with anti-PD-1 immunotherapy. The vast majority received it in combination with standard first-line chemotherapy. The anti-PD-1 inhibitors used in this cohort included nivolumab, pembrolizumab, sintilimab, tislelizumab, camrelizumab, toripalimab, and envafolimab. The chemotherapy regimens consisted of XELOX (capecitabine and oxaliplatin), SOX (S-1 and oxaliplatin), or FOLFOX (leucovorin, fluorouracil, and oxaliplatin). The choice of therapeutic regimen was determined by the treating oncologist based on contemporary clinical guidelines and the patient's individual condition. The exclusion criteria were as follows: (a) prior or planned curativeintent gastrectomy, (b) prior neoadjuvant therapy before surgery, (c) iodine contrast allergy, (d) inadequate gastrointestinal preparation leading to unclear tumor visualization, and (e) absent or poor contrast enhancement. Ultimately, 101 patients who underwent CECT before immunotherapy were included for analysis. Clinical and biochemical data were collected retrospectively. These included age, sex, hematocrit levels, and serum tumor markers, specifically carbohydrate antigen 19-9 (CA19-9) and carcinoembryonic antigen (CEA). Laboratory values were obtained from routine blood tests performed within 7 days of the CT scan. The study adhered to the principles of the Declaration of Helsinki and was approved by the Medical Ethics Committee of Wuhan Union Hospital. Written informed consent was waived due to the retrospective nature of the study.

Image acquisition

All patients provided written informed consent for abdominal CECT. Before scanning, an 8-h fasting period and iodine allergy screening were required. Abdominal imaging was performed using a 128-detector-row CT scanner (Siemens SOMATOM Definition AS+, Erlangen, Germany) with standardized parameters: tube

voltage of 120 kV, automated tube current modulation, 1.5 mm slice thickness and interval, and 512 \times 512 acquisition matrix. The patients were positioned supine, and nonionic iodinated contrast (350 mgI/mL) was administered via the antecubital vein at a flow rate of 2 to 3 mL/s. Contrast-enhanced images were acquired during the arterial phase (25–30 s post-injection), portal venous phase (50–60 s), and equilibrium phase (acquired at a fixed delay of 180 s post-injection). A research study has revealed that when estimating the ECV, the equilibrium phase at 180 s represents a good balance between the clinical workflow and technical success (24).

Image analysis

Two radiologists blinded to clinicopathological data (except tumor location) independently measured attenuation values on unenhanced CT and equilibrium-phase CECT. Regions of interest (ROIs) were manually placed within the tumor and the aorta at the same anatomical level (Figure 1). The extracellular volume fraction (ECV) was calculated using the following formula:

ECV(%) = $(1 - hematocrit) \times (\Delta HUtumor / \Delta HUaorta) \times 100$

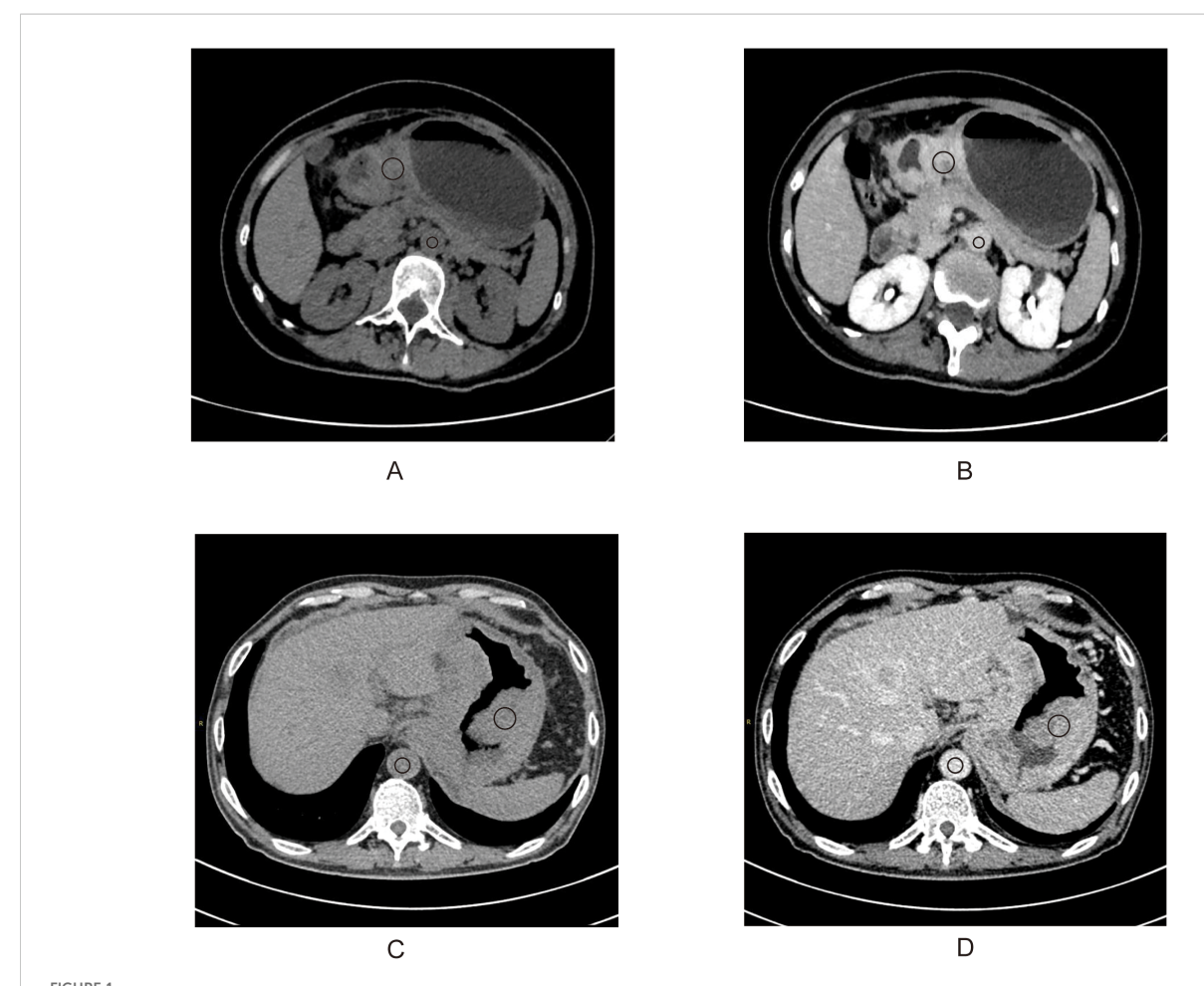
where Δ HUtumor and Δ HUaorta are the HU in the equilibrium phase minus the HU before the contrast agent administration of the tumor and the aorta, respectively (20). The final ECV value used for analysis was the average of the two radiologists' measurements.

Endpoints of the study

The primary endpoint was overall survival (OS), defined as the time from the start of immunotherapy to death or the end of follow-up in cancer patients. The secondary endpoint was progression-free survival (PFS), defined as the time from the start of treatment to disease progression or death from any cause.

Statistical analysis

To evaluate the consistency of ECV measurements between two radiologists, we employed Bland–Altman analysis and the intraclass correlation coefficient (ICC). An ICC >0.90 was considered indicative of excellent consistency (25). Using X-tile (https://medicine.yale.edu/lab/rimm/research/software/) to get the optimal



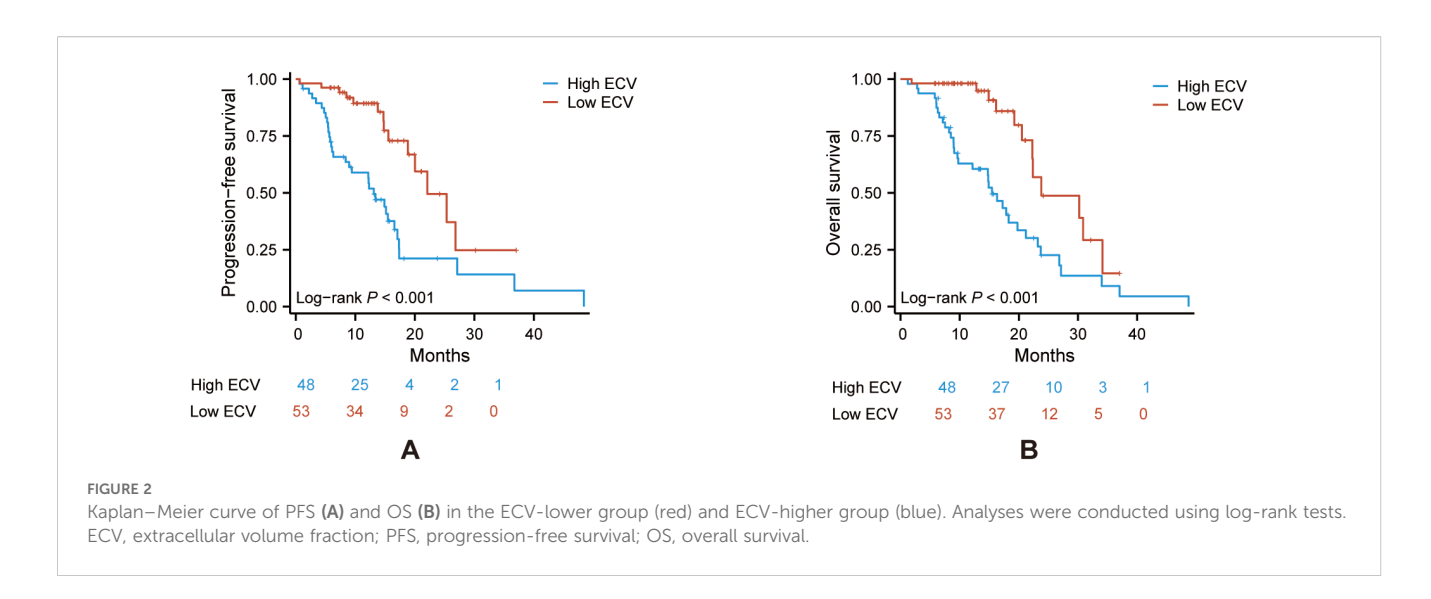
A 50-year-old woman with stage III gastric adenocarcinoma (A, B) and a 63-year-old man with stage IV gastric adenocarcinoma (C, D). Axial unenhanced (A, C); equilibrium-phase contrast-enhanced (B, D). The tumor extracellular volume fractions were 31.8% and 35.8%, respectively

TABLE 1 Baseline characteristics of patients.

Characteristics	Low-ECV group (<33.1)	High-ECV group (≥33.1)	<i>P</i> -value
Patients, n	48	53	
Age (years), n (%)			0.583
<65	13 (27.1%)	17 (32.1%)	
≥65	35 (72.9%)	36 (67.9%)	
Sex, n (%)			0.625
Female	33 (68.8%)	34 (64.2%)	
Male	15 (31.2%)	19 (35.8%)	
Clinical stage, n (%)			0.083
III	30 (62.5%)	24 (45.3%)	
IV	18 (37.5%)	29 (54.7%)	
Location, n (%)			0.200
Proximal GC	15 (31.2%)	18 (34%)	
Body GC	23 (47.9%)	17 (32.1%)	
Distal GC	10 (20.8%)	18 (34%)	
CA19-9 (U/mL), n (%)			0.956
<37	22 (45.8%)	24 (45.3%)	
≥37	26 (54.2%)	29 (54.7%)	
CEA (ng/mL), n (%)			0.091
<5	28 (58.3%)	22 (41.5%)	
≥5	20 (41.7%)	31 (58.5%)	
Smoking history, n (%)			0.452
No	38 (79.2%)	45 (84.9%)	
Yes	10 (20.8%)	8 (15.1%)	
Drinking history, n (%)			0.424
No	41 (85.4%)	48 (90.6%)	
Yes	7 (14.6%)	5 (9.4%)	
Diabetes history, n (%)			0.283
No	38 (79.2%)	37 (69.8%)	
Yes	10 (20.8%)	16 (30.2%)	
History of hypertension, n (%)			0.658
No	38 (79.2%)	40 (75.5%)	
Yes	10 (20.8%)	13 (24.5%)	
BMI, mean ± SD	21.89 ± 3.21	21.90 ± 2.53	0.986
HCT, mean ± SD	34.44 ± 4.88	33.66 ± 5.42	0.454

GC, gastric cancer; CA19-9, carbohydrate antigen 19-9; CEA, carcinoembryonic antigen; HCT, hematocrit; BMI, body mass index; mean \pm SD, mean \pm standard deviation.

cutoff values (33.1), the patients were divided into high- and low-ECV groups. X-tile employs an enumeration method that systematically tests all possible values of the continuous variable as candidate cutoff thresholds. A log-rank test was subsequently applied to compare survival curves between the stratified groups, and the cutoff point yielding the smallest p-value was selected as the optimal threshold (26). Normally distributed continuous variables were compared using Student's t-test and expressed as mean \pm standard deviation (SD). Categorical variables were analyzed via chi-square or Fisher's exact tests and reported as percentages (n, %).



The PFS and OS between the high- and low-ECV groups were compared using log-rank test and visualized with Kaplan-Meier curves. Univariate and multivariate Cox regression analyses identified prognostic factors, with variables showing p < 0.05 in univariate analysis included in the multivariate model. The results were reported as hazard ratios (HRs) with 95% confidence intervals (CIs). Subgroup analyses were conducted to explore the consistency of the ECV effect. Two predictive models were constructed: model 1 included clinical stage, age group, and sex, while model 2 encompassed all variables from model 1 plus ECV stratification. The predictive performance was evaluated using ROC curves and AUC. Internal validation of AUC values was conducted using a bootstrap resampling method with 1,000 iterations. Statistical significance was defined as p < 0.05. Analyses were performed using SPSS 27.0 (IBM Corp.) and R 4.4.2 (R Foundation for Statistical Computing).

Results

Interobserver agreement of ECV measurements

The Bland–Altman analysis demonstrated excellent agreement between two radiologists in CT-ECV quantification (Supplementary Figure S1). The mean bias was 0.82 units (95% CI: 0.12–1.53), with 95% limits of agreement (LoA) ranging from -6.20 to +7.85. Approximately 95% of data points fell within the LoA, confirming high measurement reproducibility. This was further supported by an ICC of 0.971 (95% CI: 0.957–0.981) for average measures, indicating good consistency.

Patients' baseline characteristics

A total of 101 gastric adenocarcinoma patients were included in this study. The average age was 59.3 ± 11.9 years, with 66% being male. Based on the ECV indices and using X-tile, the optimal cutoff

values were determined (33.1). There were 48 patients in the low-ECV group (<33.1) and 53 patients in the high-ECV group (≥33.1). No significant differences were observed in age, sex distribution, clinical stage, tumor location, tumor markers, HCT, BMI, risk factors, or other comorbidities (Table 1).

Survival analysis

Kaplan–Meier survival curves of PFS and OS were conducted between the two groups. The log-rank tests indicated that the ECV-higher group had a shorter PFS (P < 0.001) and OS (P < 0.001) than the ECV-lower group (Figures 2A, B).

Cox regression analysis and subgroup analysis

Univariate analysis showed that high ECV significantly predicted a shorter progression-free survival (PFS: HR = 3.194, 95% CI: 1.702–5.993, P < 0.001), and clinical stage IV was associated with reduced PFS (HR = 3.078, 95% CI: 1.660–5.707, P < 0.001). For OS, high ECV and clinical stage IV showed a stronger prognostic value (HR = 3.220, 95% CI: 1.665–6.230, P < 0.001; HR = 3.501, 95% CI: 1.872–6.549, P < 0.001).

Multivariate analysis showed that high ECV independently predicted shorter PFS (HR = 2.716, 95% CI: 1.432-5.152, P=0.002) and OS (HR = 2.593, 95% CI: 1.322-5.084, P=0.006). Similarly, clinical stage IV remained significantly linked to both shorter PFS (HR = 2.573, 95% CI: 1.377-4.808, P=0.003) and poorer OS (HR = 2.881, 95% CI: 1.524-5.448, P=0.001) (Tables 2, 3).

We performed a subgroup analysis of patients based on baseline characteristics and observed relatively consistent results for PFS and OS, and the hazard ratios for each subgroup were derived from the univariate Cox model. Forest plots revealed a uniformly increased risk in high-ECV patients across all subgroups, both in PFS and OS (Figures 3, 4). The association between high ECV and worse

TABLE 2 Univariate and multivariate Cox proportional hazards analyses for PFS.

Characteristics	Total (A)	Univariate an	Univariate analysis		nalysis
	Total (N)	Hazard ratio (95% CI)	<i>P</i> -value	Hazard ratio (95% CI)	<i>P</i> -value
Sex	101				
Female	34	Reference			
Male	67	1.084 (0.587-2.001)	0.797		
Age	101				
<65 years	71	Reference			
≥65 years	30	1.297 (0.644-2.614)	0.467		
Clinical stage	101				
III	47	Reference		Reference	
IV	54	3.078 (1.660–5.707)	<0.001	2.573 (1.377–4.808)	0.003
Location	101				
Proximal GC	33	Reference			
Body GC	40	1.617 (0.804–3.252)	0.178		
Distal GC	28	1.260 (0.578-2.748)	0.561		
CA19-9	101				
<37 (U/mL)	55	Reference			
≥37 (U/mL)	46	1.273 (0.718–2.258)	0.409		
CEA	101				
<5 (ng/mL)	50	Reference			
≥5 (ng/mL)	51	1.225 (0.677–2.216)	0.503		
Smoking history	101				
No	83	Reference			
Yes	18	1.372 (0.674–2.796)	0.383		
Drinking history	101				
No	89	Reference			
Yes	12	1.366 (0.573–3.257)	0.481		
Diabetes history	101				
No	75	Reference			
Yes	26	1.319 (0.620-2.808)	0.472		
History of hypertension	101				
No	78	Reference			
Yes	23	0.508 (0.229–1.128)	0.096		
ECV group	101				
Low	53	Reference		Reference	
High	48	3.194 (1.702–5.993)	<0.001	2.716 (1.432–5.152)	0.002

PFS, progression-free survival; CI, confidence interval; GC, gastric cancer; CA19-9, carbohydrate antigen 19-9; CEA, carcinoembryonic antigen; ECV, extracellular volume fraction.

TABLE 3 Univariate and multivariate Cox proportional hazards analyses for OS.

Characteristics	Total (<i>N</i>)	Univariate ar	nalysis	Multivariate ar	nalysis
		Hazard ratio (95% CI)	P-value	Hazard ratio (95% CI)	P-value
Sex	101				
Female	34	Reference			
Male	67	1.211 (0.642-2.285)	0.554		
Age	101				
<65 years	71	Reference			
≥65 years	30	1.429 (0.726–2.814)	0.301		
Clinical stage	101				
III	47	Reference		Reference	
IV	54	3.501 (1.872–6.549)	<0.001	2.881 (1.524–5.448)	0.001
Location	101				
Proximal GC	33	Reference			
Body GC	40	1.911 (0.941-3.883)	0.073		
Distal GC	28	1.612 (0.736–3.535)	0.233		
CA19-9	101				
<37 (U/mL)	55	Reference			
≥37 (U/mL)	46	1.356 (0.757-2.429)	0.305		
CEA	101				
<5 (ng/mL)	50	Reference			
≥5 (ng/mL)	51	0.996 (0.551-1.801)	0.991		
Smoking history	101				
No	83	Reference			
Yes	18	1.548 (0.782–3.066)	0.210		
Drinking history	101				
No	89	Reference			
Yes	12	1.551 (0.643-3.739)	0.328		
Diabetes history	101				
No	75	Reference			
Yes	26	1.680 (0.733–3.851)	0.220		
History of hypertension	101				
No	78	Reference			
Yes	23	0.678 (0.322-1.428)	0.307		
ECV group	101				
Low	53	Reference		Reference	
High	48	3.220 (1.665–6.230)	<0.001	2.593 (1.322–5.084)	0.006

OS, overall survival; CI, confidence interval; GC, gastric cancer; CA19-9, carbohydrate antigen 19-9; CEA, carcinoembryonic antigen; ECV, extracellular volume fraction.

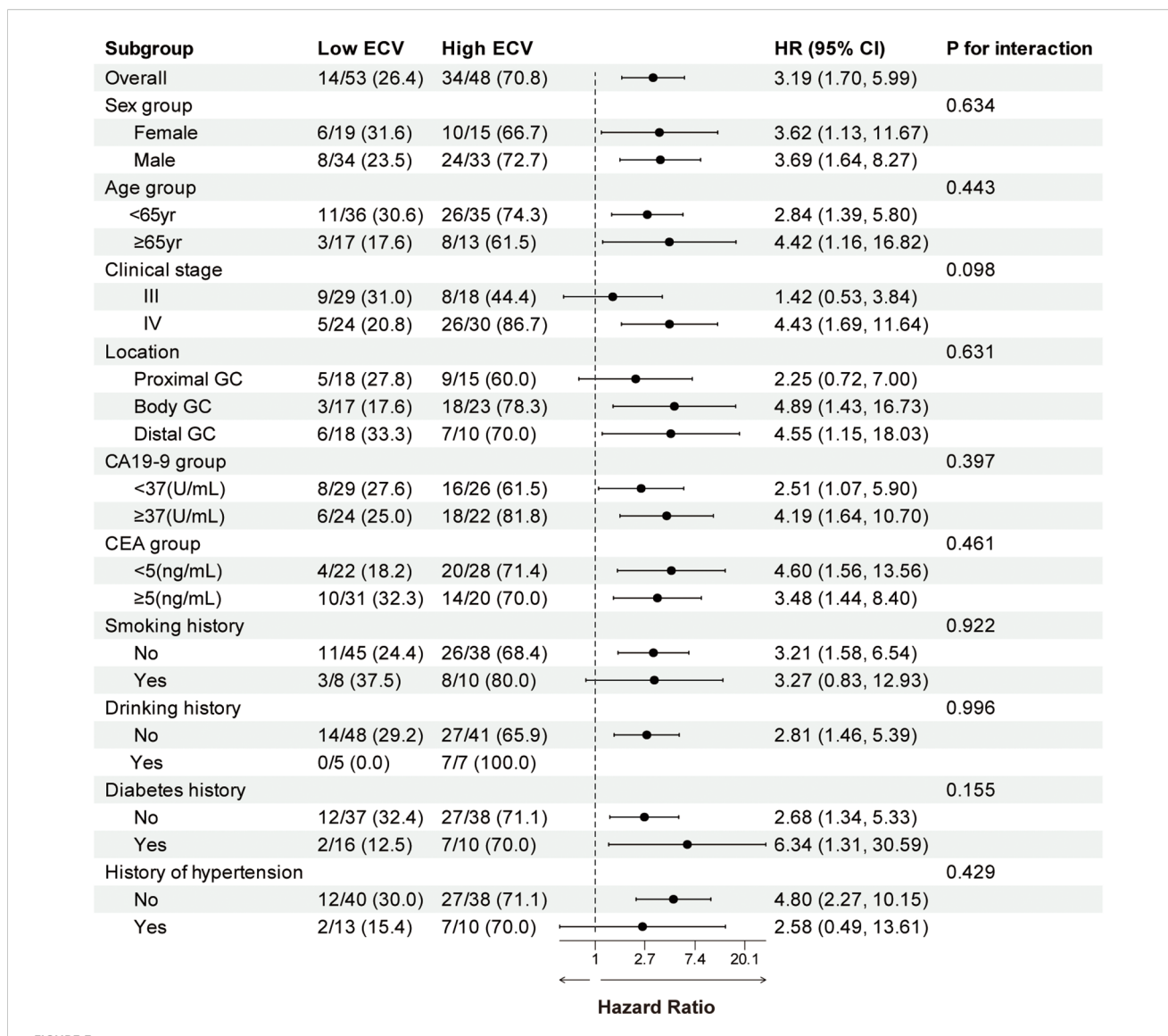


FIGURE 3
Forest plot of subgroup analysis in progression-free survival between the ECV-lower group and ECV-higher group. The dashed line indicates a hazard ratio of 1. ECV, extracellular volume fraction; HR, hazard ratio; CI, confidence interval; GC, gastric cancer; CA19-9, carbohydrate antigen 19-9; CEA, carcinoembryonic antigen.

survival was consistent within both stage III and stage IV subgroups. No significant heterogeneity of ECV effect was observed (all P for interaction >0.05), supporting the robustness of ECV as a universal predictor.

Combination of multiple indicators for predicting disease progression and survival outcomes

ROC curves demonstrated the predictive ability at 1-year survival rate of the combination of clinical stage with ECV for PFS and OS. For PFS prediction (Figure 5A), the combined model (model 2: clinical stage, age group, sex, and ECV group) demonstrated superior discriminative ability compared to model 1 (clinical stage, age group, and sex), with AUC values of 0.739 (95%)

CI: 0.614-0.865) versus 0.712 (95% CI: 0.587-0.836). Similarly, in OS prediction (Figure 5B), the integration of ECV (model 2) significantly improved predictive accuracy compared to model 1, demonstrated by an increase in AUC from 0.736 (95% CI: 0.588-0.885) to 0.806 (95% CI: 0.697-0.914). To further assess the robustness and internal validity of the prognostic models, we performed bootstrap resampling (B = 1,000) to estimate the timedependent AUCs and their 95% CIs at 1-year follow-up. Internal validation of the ROC curves was performed using bootstrap resampling with 1,000 iterations. The internally validated results consistently confirmed the superior performance of model 2 compared to model 1 (Supplementary Figures S2, S3). For OS prediction, the 1-year AUC of model 1 was 0.772 (95% CI: 0.636-0.892); for model 2, the 1-year AUC was 0.835 (95% CI: 0.728-0.932). For PFS prediction, the 1-year AUC of model 1 was 0.734 (95% CI: 0.611-0.848); for model 2, the 1-year AUC was 0.774 (95%

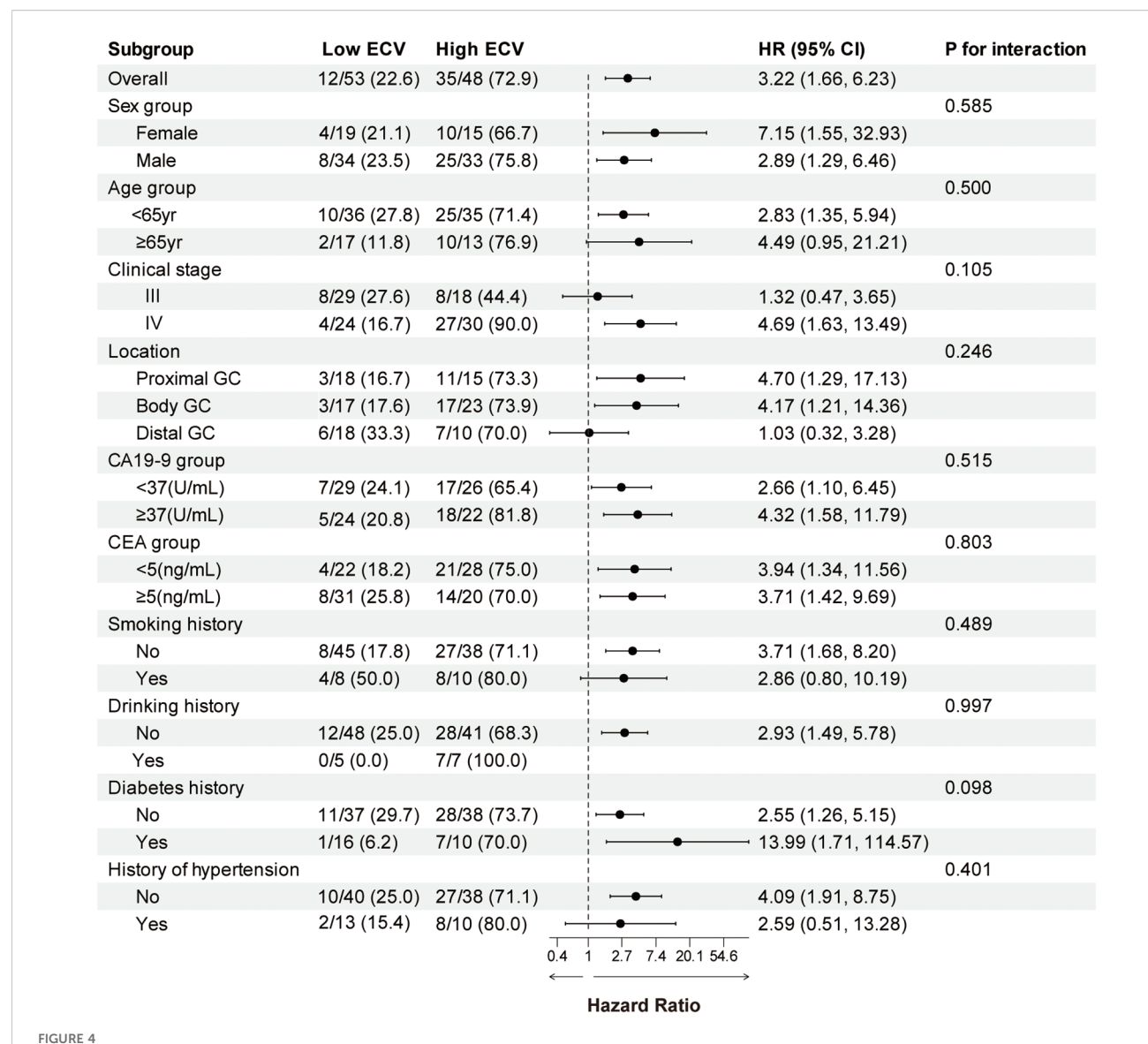


FIGURE 4 Forest plot of subgroup analysis in overall survival between the ECV-lower group and ECV-higher group. The dashed line indicates a hazard ratio of 1. ECV, extracellular volume fraction; HR, hazard ratio; CI, confidence interval; GC, gastric cancer; CA19-9, carbohydrate antigen 19-9; CEA, carcinoembryonic antigen.

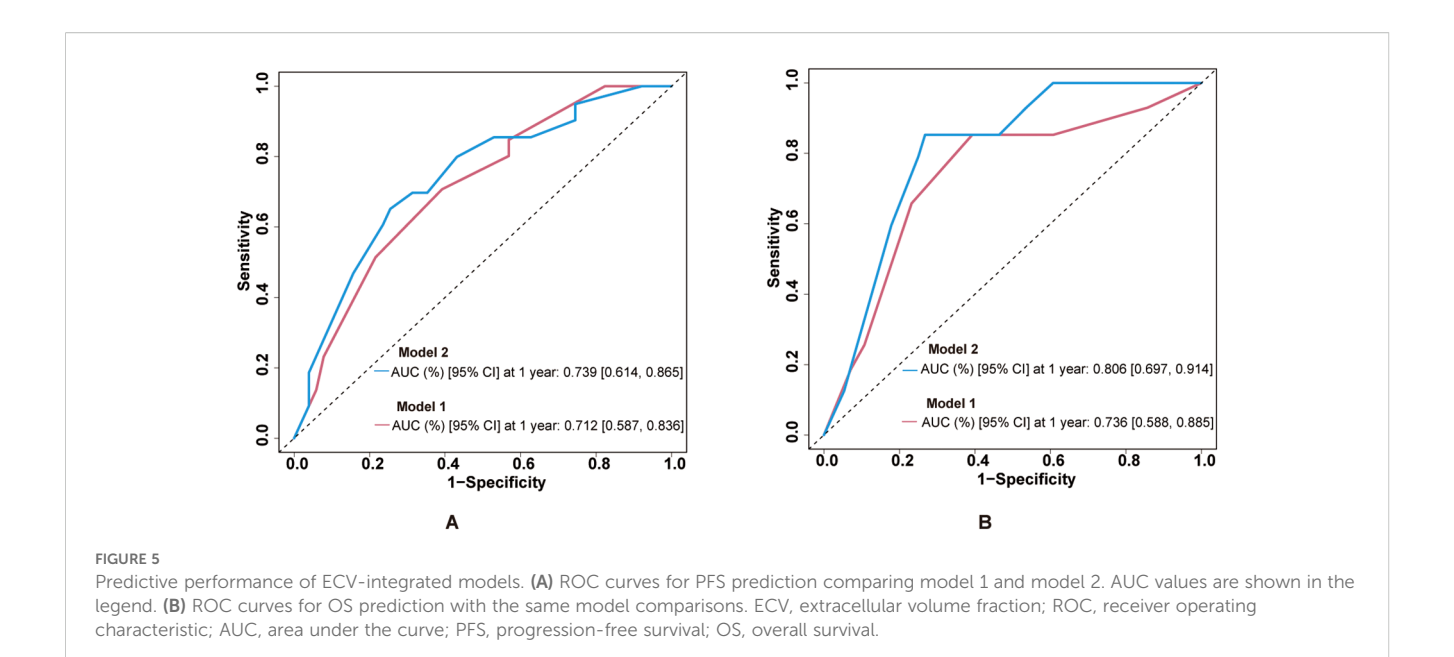
CI: 0.646–0.886). These findings suggest that the inclusion of ECV enhanced the discriminative ability of the clinical model and that the results remained stable after internal validation using bootstrap methods.

Discussion

ECV has traditionally been used to assess fibrosis in organs such as the heart, liver, and pancreas (10, 12, 13), but its role in gastric cancer has rarely been explored. In this retrospective study, we were the first to investigate the prognostic value of ECV in gastric cancer patients receiving immunotherapy. Multivariate Cox regression analysis, which adjusted for the influence of clinical stage, confirmed that high CT-ECV was independently associated with worse PFS (HR = 2.716, 95%

CI: 1.432–5.152, P = 0.002) and OS (HR = 2.593, 95% CI: 1.322–5.084, P = 0.006). Moreover, integrating ECV into a clinical-stage-based prognostic model improved its predictive performance. The combined model demonstrated higher area under the ROC curve values (PFS: AUC = 0.739, 95% CI: 0.614–0.865; OS: AUC = 0.806, 95% CI: 0.697–0.914), supporting the added prognostic value of ECV. Internal validation using bootstrap resampling (B = 1,000) confirmed the consistency and robustness of the combined model, further reinforcing the credibility of our findings. Collectively, these results suggest that ECV may serve as a noninvasive imaging biomarker, with potential utility in predicting immunotherapy outcomes.

Of the existing biomarkers for gastric cancer immunotherapy, such as PD-L1 expression, MSI, tumor mutational burden (TMB), EBV status, liquid biopsy, and emerging multi-omics approaches, many have significantly improved the precision of predicting



immunotherapy efficacy. However, the clinical utility of these biomarkers is constrained by several factors, including spatial and temporal heterogeneity, sampling bias, invasiveness of tissue acquisition, dynamic changes in PD-L1 expression, the high cost and technical complexity associated with genomic profiling like TMB, as well as the poor interpretability and inherent complexity of radiomics models (27). Even emerging non-invasive methods such as liquid biopsy face challenges related to sensitivity, specificity, and the potential for false-positive results (28). In contrast, the CT-ECV framework evaluated in this study utilizes standard contrastenhanced CT scans, making it a non-invasive, readily accessible, and cost-effective tool. More importantly, ECV provides unique biological insight by directly quantifying a fundamental and functionally critical aspect of the tumor microenvironment (TME)—the fibrotic extracellular matrix (ECM). As our results and the discussed mechanisms suggest, a high ECV likely reflects a stroma-rich, immunosuppressive TME characterized by dense physical barriers that impede immune cell infiltration and drug delivery (29). Therefore, although ECV, like any novel biomarker, requires further validation in larger cohorts, it is not intended to replace existing markers but rather to serve as a highly practical and complementary biomarker.

Increased stiffness of the ECM is considered a key factor in promoting an immunosuppressive tumor microenvironment. It can stimulate M2 macrophage polarization through mechanotransduction pathways and induce the release of immunosuppressive cytokines. Additionally, ECM stiffening contributes to tissue hypoxia and activates the HIF- α signaling pathway, collectively leading to an immunosuppressive and T-cell-exhausted microenvironment. Furthermore, the dense structure of the ECM not only forms a physical barrier that limits immune cell infiltration into the tumor but also exerts mechanical tension that activates mechanosensitive signaling pathways. As a result, T-cell migration is restricted, and anti-PD-1 antibodies may have difficulty penetrating into the tumor core, ultimately compromising the efficacy of immunotherapy (30–32).

The tumor microenvironment, particularly the stromal component, plays a crucial part in GC progression. Previous studies have demonstrated that tumor-associated stroma plays an active role in tumor invasion and metastasis and that GC with high stromal content are associated with worse prognosis compared to those with low stromal content (33-35). Moreover, it has been reported that collagen density modulates the activity of tumor-infiltrating T cells, with high collagen density leading to reduced T-cell proliferation and impaired cytotoxic function, ultimately promoting immune escape by tumor cells (36). Consistent with previous findings in postoperative gastric cancer, elevated CT-derived ECV has been shown to reflect stromal-rich tumor microenvironments that may facilitate tumor progression and resistance (23). Our study extends this concept into the immunotherapy setting. ECV, a noninvasive imaging biomarker, serves as an indirect indicator of the amount and spatial distribution of ECM within the tumor tissue, which may explain the poorer prognosis observed in patients with high ECV undergoing immunotherapy (9). Interestingly, in some cancers such as pancreatic adenocarcinoma, higher ECV has been associated with better drug distribution and longer survival (16, 37). These divergent associations may be explained by fundamental differences in the biological nature of the tumor stroma across cancer types coupled with the distinct mechanisms of action of different therapeutic regimens. We propose that this paradox hinges on a fundamental question: does the treatment strategy actively attack the stromal barrier, or must it bypass it? In pancreatic cancer, cornerstone chemotherapies (e.g., nab-paclitaxel plus gemcitabine) function as stroma-depleting agents, physically breaking down the fibrotic barrier (38). Here a high baseline ECV may simply mark a larger, more susceptible target for chemotherapy regimen. However, in the context of immunotherapy, this phenomenon does not necessarily translate into improved therapeutic outcomes. PD-1 inhibitors do not dismantle the barrier but require T-cells to traverse it. Thus, an elevated ECV may indicate a denser stromal architecture, restricted T-cell migration, and enhanced immunosuppression, which could counteract the potential benefits of increased drug dispersion. This comparison highlights that

ECV quantifies a dynamic interface whose impact is determined by the therapy applied. These findings suggest that further mechanistic studies and external validation are warranted in diverse cancer types and immune phenotypes to better understand the complex relationship between ECV and immunotherapy response.

This study has several limitations. First, being a retrospective single-center study, the findings may be subject to selection bias and limited generalizability despite the use of strict inclusion criteria. Second, the relatively small sample size restricted the statistical power of some subgroup analyses, although we performed internal validation using bootstrap methods to enhance reliability. Third, ECV was measured based on conventional single-energy CT rather than dual-energy or spectral CT, which may introduce variability; however, standardized imaging protocols and ROI selection helped minimize this issue. Lastly, external validation in independent cohorts was not conducted, and prospective multicenter studies are warranted to confirm the generalizability and clinical applicability of our model. In conclusion, CT-derived ECV may serve as an independent prognostic factor in gastric cancer patients treated with immunotherapy. As a noninvasive imaging biomarker, ECV holds promise for risk stratification and therapeutic decisionmaking in this patient population and warrants further validation in clinical practice.

Conclusion

This retrospective cohort study of gastric cancer patients undergoing immunotherapy demonstrated that contrast-enhanced CT-derived ECV may serve as an independent predictor for both PFS and OS patients with low ECV who exhibited improved PFS and OS compared to those with high ECV.

Data availability statement

The raw data supporting the conclusions of this article will be made available by the authors, without undue reservation.

Ethics statement

The studies involving humans were approved by Ethics Committee of Union Hospital, Tongji Medical College, Huazhong University of Science and Technology. The studies were conducted in accordance with the local legislation and institutional requirements. Written informed consent for participation was not required from the participants or the participants' legal guardians/next of kin in accordance with the national legislation and institutional requirements.

Author contributions

YYW: Formal analysis, Writing – original draft, Conceptualization, Software. SSJ: Software, Data curation, Formal analysis, Writing –

original draft. YJY: Data curation, Formal analysis, Writing – original draft, Software. YL: Data curation, Writing – original draft, Investigation. ZYL: Data curation, Writing – original draft, Investigation. ZQL: Supervision, Writing – review & editing, Visualization. XCK: Supervision, Writing – review & editing, Visualization. GFZ: Visualization, Supervision, Conceptualization, Writing – review & editing.

Funding

The author(s) declare that no financial support was received for the research, and/or publication of this article.

Acknowledgments

We are profoundly grateful to the clinical investigators and study participants whose crucial contributions have been instrumental in driving this scientific project forward.

Conflict of interest

The authors declare that the research was conducted in the absence of any commercial or financial relationships that could be construed as a potential conflict of interest.

Generative AI statement

The author(s) declare that no Generative AI was used in the creation of this manuscript.

Any alternative text (alt text) provided alongside figures in this article has been generated by Frontiers with the support of artificial intelligence and reasonable efforts have been made to ensure accuracy, including review by the authors wherever possible. If you identify any issues, please contact us.

Publisher's note

All claims expressed in this article are solely those of the authors and do not necessarily represent those of their affiliated organizations, or those of the publisher, the editors and the reviewers. Any product that may be evaluated in this article, or claim that may be made by its manufacturer, is not guaranteed or endorsed by the publisher.

Supplementary material

The Supplementary Material for this article can be found online at: https://www.frontiersin.org/articles/10.3389/fonc.2025.1698065/full#supplementary-material

References

- 1. Tan N, Wu H, Cao M, Yang F, Yan X, He S, et al. Global, regional, and national burden of early-onset gastric cancer. *Cancer Biol Med.* (2024) 21:667–78. doi: 10.20892/i.issn.2095-3941.2024.0159
- 2. Guan WL, He Y, Xu RH. Gastric cancer treatment: recent progress and future perspectives. J Hematol Oncol. (2023) 16:57. doi: 10.1186/s13045-023-01451-3
- 3. Theocharis AD, Skandalis SS, Gialeli C, Karamanos NK. Extracellular matrix structure. Adv Drug Del Rev. (2016) 97:4–27. doi: 10.1016/j.addr.2015.11.001
- 4. Moreira AM, Pereira J, Melo S, Fernandes MS, Carneiro P, Seruca R, et al. The extracellular matrix: an accomplice in gastric cancer development and progression. *Cells.* (2020) 9:394. doi: 10.3390/cells9020394
- 5. Bonnans C, Chou J, Werb Z. Remodelling the extracellular matrix in development and disease. *Nat Rev Mol Cell Biol.* (2014) 15:786–801. doi: 10.1038/nrm3904
- 6. Mouw JK, Ou G, Weaver VM. Extracellular matrix assembly: a multiscale deconstruction. *Nat Rev Mol Cell Biol.* (2014) 15:771–85. doi: 10.1038/nrm3902
- 7. Fleming JM, Yeyeodu ST, McLaughlin A, Schuman D, Taylor DK. *In situ* drug delivery to breast cancer-associated extracellular matrix. *ACS Chem Biol.* (2018) 13:2825–40. doi: 10.1021/acschembio.8b00396
- 8. Majo S, Courtois S, Souleyreau W, Bikfalvi A, Auguste P. Impact of extracellular matrix components to renal cell carcinoma behavior. *Front Oncol.* (2020) 10:625. doi: 10.3389/fonc.2020.00625
- 9. Gerber BL. Assessment of the extracellular matrix by CT extracellular volume fraction. *JACC Cardiovasc Imag.* (2024) 17:529–32. doi: 10.1016/j.jcmg.2023.11.011
- 10. Nacif MS, Kawel N, Lee JJ, Chen X, Yao J, Zavodni A, et al. Interstitial myocardial fibrosis assessed as extracellular volume fraction with low-radiation-dose cardiac CT. *Radiology*. (2012) 264:876–83. doi: 10.1148/radiol.12112458
- Chen Y, Jiang J, Yan C, Jiang J, Shi B, Xu Z, et al. Prediction of tumor regression grade in far-advanced gastric cancer after preoperative immuno-chemotherapy using dual-energy CT-derived extracellular volume fraction. *Eur Radiol.* (2025) 35:93–104. doi: 10.1007/s00330-024-10737-0
- 12. Tago K, Tsukada J, Sudo N, Shibutani K, Okada M, Abe H, et al. Comparison between CT volumetry and extracellular volume fraction using liver dynamic CT for the predictive ability of liver fibrosis in patients with hepatocellular carcinoma. *Eur Radiol.* (2022) 32:7555–65. doi: 10.1007/s00330-022-08852-x
- Sofue K, Ueshima E, Masuda A, Shirakawa S, Zen Y, Ueno Y, et al. Estimation of pancreatic fibrosis and prediction of postoperative pancreatic fistula using extracellular volume fraction in multiphasic contrast-enhanced CT. Eur Radiol. (2022) 32:1770–80. doi: 10.1007/s00330-021-08255-4
- 14. Lohi J, Leivo I, Oivula J, Lehto VP, Virtanen I. Extracellular matrix in renal cell carcinomas. *Histol Histopathol.* (1998) 13:785–96. doi: 10.14670/HH-13.785
- 15. Luo Y, Liu L, Liu D, Shen H, Wang X, Fan C, et al. Extracellular volume fraction determined by equilibrium contrast-enhanced CT for the prediction of the pathological complete response to neoadjuvant chemoradiotherapy for locally advanced rectal cancer. *Eur Radiol.* (2023) 33:4042–51. doi: 10.1007/s00330-022-09307-z
- 16. Fukukura Y, Kumagae Y, Higashi R, Hakamada H, Takumi K, Maemura K, et al. Extracellular volume fraction determined by equilibrium contrast-enhanced multidetector computed tomography as a prognostic factor in unresectable pancreatic adenocarcinoma treated with chemotherapy. *Eur Radiol.* (2019) 29:353–61. doi: 10.1007/s00330-018-5570-4
- 17. Iwaya H, Fukukura Y, Hashimoto S, Tanoue S, Kawahira M, Hinokuchi M, et al. Prognostic significance of extracellular volume fraction with equilibrium contrastenhanced computed tomography for pancreatic neuroendocrine neoplasms. *Pancreatology.* (2021) 21:779–86. doi: 10.1016/j.pan.2021.02.020
- 18. Jiang X, Ma Q, Zhou T, Feng Q, Yang W, Zhou X, et al. Extracellular volume fraction as a potential predictor to differentiate lung cancer from benign lung lesions with dual-layer detector spectral CT. *Quant Imaging Med Surg.* (2023) 13:8121–31. doi: 10.21037/qims-23-736
- 19. Yoshida K, Yamaguchi K, Okumura N, Tanahashi T, Kodera Y. Is conversion therapy possible in stage IV gastric cancer: the proposal of new biological categories of classification. *Gastric Can.* (2016) 19:329–38. doi: 10.1007/s10120-015-0575-z

- 20. Nishimuta Y, Tsurumaru D, Fujita N, Kai S, Maehara J, Ushijima Y, et al. CT-derived extracellular volume fraction as a predictive marker for postoperative recurrence in pStage II–III gastric cancer. *Eur Radiol.* (2025). Available at: https://doi.org/10.1007/s00330-025-11765-0.
- 21. Liu Y, Li C, Lu Y, Liu C, Yang W. Tumor microenvironment-mediated immune tolerance in development and treatment of gastric cancer. *Front Immunol.* (2022) 13:1016817. doi: 10.3389/fimmu.2022.1016817
- 22. Chen Y, Jiang J, Yan C, Jiang J, Shi B, Xu X, et al. Prediction of tumor regression grade in far-advanced gastric cancer after preoperative immuno-chemotherapy using dual-energy CT-derived extracellular volume fraction. *Eur Radiol.* (2025) 35(1):93–104. doi: 10.1038/bic.2013.415
- 23. Yusuke N, Daisuke T, Nobuhiro F, Satohiro K, Junki M, Yasuhiro U, et al. CT-derived extracellular volume fraction as a predictive marker for postoperative recurrence in pStage II–III gastric cancer. *Eur Radiol.* (2025). doi: 10.1007/s00330-025-11765-0
- 24. Yoon JH, Lee JM, Klotz E, Jeon JH, Lee KB, Han JK, et al. Estimation of hepatic extracellular volume fraction using multiphasic liver computed tomography for hepatic fibrosis grading. *Invest Radiol.* (2015) 50:290. doi: 10.1097/RLI.0000000000000123
- 25. Benchoufi M, Matzner-Lober E, Molinari N, Jannot AS, Soyer P. Interobserver agreement issues in radiology. *Diagn Intervent Imag.* (2020) 101:639–41. doi: 10.1016/j.diii.2020.09.001
- 26. Camp RL, Dolled-Filhart M, Rimm DL. X-tile: a new bio-informatics tool for biomarker assessment and outcome-based cut-point optimization. *Clin Cancer Res.* (2004) 10:7252–9. doi: 10.1158/1078-0432.CCR-04-0713
- 27. Hou W, Zhao Y, Zhu H. Predictive biomarkers for immunotherapy in gastric cancer: current status and emerging prospects. *Int J Mol Sci.* (2023) 24:15321. doi: 10.3390/ijms242015321
- 28. Nikanjam M, Kato S, Kurzrock R. Liquid biopsy: current technology and clinical applications. *J Hematol Oncol.* (2022) :15:131. doi: 10.1186/s13045-022-01351-y
- 29. Prakash J, Shaked Y. The interplay between extracellular matrix remodeling and cancer therapeutics. *Cancer Discov.* (2024) 14:1375–88. doi: 10.1158/2159-8290.CD-24-0002
- 30. Yuan Z, Li Y, Zhang S, Wang X, Dou H, Yu X, et al. Extracellular matrix remodeling in tumor progression and immune escape: from mechanisms to treatments. *Mol Can.* (2023) 22:48. doi: 10.1186/s12943-023-01744-8
- 31. Naik A, Leask A. Tumor-associated fibrosis impairs the response to immunotherapy. *Matrix Biol.* (2023) 119:125–40. doi: 10.1016/j.matbio.2023.04.002
- 32. Brahimi-Horn MC, Chiche J, Pouysségur J. Hypoxia and cancer. J Mol Med. (2007) 85:1301–7. doi: 10.1007/s00109-007-0281-3
- 33. Aurello P, Berardi G, Giulitti D, Palumbo A, Tierno SM, Nigri G, et al. Tumor-Stroma Ratio is an independent predictor for overall survival and disease free survival in gastric cancer patients. *Surgeon.* (2017) 15:329–35. doi: 10.1016/j.surge.2017.05.007
- 34. Peng C, Liu J, Yang G, Li Y. The tumor-stromal ratio as a strong prognosticator for advanced gastric cancer patients: proposal of a new TSNM staging system. *J Gastroenterol.* (2018) 53:606–17. doi: 10.1007/s00535-017-1379-1
- 35. Wu J, Liang C, Chen M, Su W. Association between tumor-stroma ratio and prognosis in solid tumor patients: a systematic review and meta-analysis. *Oncotarget*. (2016) 7:68954–65. doi: 10.18632/oncotarget.12135
- 36. Kuczek DE, Larsen AMH, Thorseth ML, Carretta M, Kalvisa A, Siersbæk MS, et al. Collagen density regulates the activity of tumor-infiltrating T cells. *J immunother Can.* (2019) 7:68. doi: 10.1186/s40425-019-0556-6
- 37. Fukukura Y, Kumagae Y, Higashi R, Hakamada H, Nakajo M, Maemura K, et al. Extracellular volume fraction determined by equilibrium contrast-enhanced dual-energy CT as a prognostic factor in patients with stage IV pancreatic ductal adenocarcinoma. *Eur Radiol.* (2020) 30:1679–89. doi: 10.1007/s00330-019-06517-w
- 38. Alvarez R, Musteanu M, Garcia-Garcia E, Lopez-Casas PP, Megias D, Guerra C, et al. Stromal disrupting effects of nab-paclitaxel in pancreatic cancer. *Br J Can.* (2013) 109:926–33. doi: 10.1038/bjc.2013.415